Global Biogeochemical Cycles

RESEARCH ARTICLE
10.1029/2018GB005948

Isotopic Constraints on Nitrogen Transformation Rates in the Deep Sedimentary Marine Biosphere

C. Buchwald[1,2], K. Homola[3], A. J. Spivack[3], E. R. Estes[1], R. W. Murray[4], and S. D. Wankel[1]

[1]Marine Chemistry and Geochemistry Department, Woods Hole Oceanographic Institution, Woods Hole, MA, USA, [2]Department of Oceanography, Dalhousie University, Halifax, Nova Scotia, Canada, [3]School of Oceanography, University of Rhode Island, Narragansett, RI, USA, [4]Earth and Environment, Boston University, Boston, MA, USA

Key Points:
- N and O stable isotope profiles reflect a combination of nitrogen cycling processes in deep-sea sediments
- Reaction-diffusion modeling suggests an unusual dynamic between N isotopes of NO_3^- and NO_2^-, with a number of possible mechanisms discussed

Correspondence to:
C. Buchwald & S. D. Wankel,
cbuchwald@dal.ca;
sdwankel@whoi.edu

Citation:
Buchwald, C., Homola, K., Spivack, A. J., Estes, E. R., Murray, R. W., & Wankel, S. D. (2018). Isotopic constraints on nitrogen transformation rates in the deep sedimentary marine biosphere. *Global Biogeochemical Cycles*, *32*, 1688–1702. https://doi.org/10.1029/2018GB005948

Received 5 APR 2018
Accepted 1 OCT 2018
Accepted article online 18 OCT 2018
Published online 26 NOV 2018

Abstract Little is known about the nature of microbial community activity contributing to the cycling of nitrogen in organic-poor sediments underlying the expansive oligotrophic ocean gyres. Here we use pore water concentrations and stable N and O isotope measurements of nitrate and nitrite to constrain rates of nitrogen cycling processes over a 34-m profile from the deep North Atlantic spanning fully oxic to anoxic conditions. Using a 1-D reaction-diffusion model to predict the distribution of nitrogen cycling rates, results converge on two distinct scenarios: (1) an exceptionally high degree of coupling between nitrite oxidation and nitrate reduction near the top of the anoxic zone or (2) an unusually large N isotope effect (~60‰) for nitrate reduction that is decoupled from the corresponding O isotope effect, which is possibly explained by enzyme-level *interconversion* between nitrite and nitrate.

1. Introduction

Sediments underlying the oligotrophic ocean gyres comprise the vast majority of the seafloor yet remain far less examined than the sediments of the coastal and continental shelf zones. Indeed, our understanding of the distribution, magnitude, and controls on elemental cycling occurring in these deep sea sediments is still in its infancy (Schrenk et al., 2010). The relatively low organic carbon input and low sedimentation rates that typify the majority of the global ocean greatly reduce respiratory consumption of O_2 (and other electron acceptors such as nitrate [NO_3^-]), allowing oxic conditions to penetrate deeply (greater than tens of meters; D'Hondt et al., 2015; Orcutt et al., 2013; Ziebis et al., 2012). Indeed, these slower microbial respiration rates are consistent with the dramatically lower abundances and activities of microbial communities in these regions. Our understanding of the nature of these microbial communities, however, is limited, in part by the challenges of studying microbial activity at such low cell abundances (D'Hondt et al., 2004, 2009, 2015). It often remains difficult to determine which processes occur and at what rates—greatly limiting our understanding of life under these ubiquitous conditions (D'Hondt et al., 2004).

Vertical profiles of solute concentrations are frequently used in both sedimentary pore waters and water column settings to infer the distribution and magnitude of respiration pathways and rates (Berner, 1964, 1980; D'Hondt et al., 2004; Froelich et al., 1979). For example, the pore water distribution of nitrate reflects the vertical distribution of net nitrate production (via nitrification) and consumption (via denitrification). Interpreting concentration profiles with reaction-diffusion models allows estimation of production and consumption rates (Berner, 1980; Boudreau, 1997; Wang et al., 2008). Such approaches have enabled powerful insights into the magnitude and distribution of microbial reactions occurring over a wide range of sediment environments. Additionally, these studies are useful because they are noninvasive and estimate the magnitude of cycling processes under in situ conditions. New techniques, including isotope labeling incubations as well as metagenomic and metatranscriptomic approaches, indicate that the network of operative microbial metabolic reactions is often far more complex than previously believed and may include an abundance of more *cryptic* reactions (Canfield et al., 2010; Kappler & Bryce, 2017; Orsi et al., 2013; Riedinger et al., 2017). A commonality among these cryptic reactions is the rapid turnover of a reactive intermediate, which is often undetectable in the environment (e.g., Canfield et al., 2010; Hansel et al., 2015; Ward & Zafiriou, 1988); the balance of oxidative and reductive processes keeps steady state concentrations of these intermediates low. Reactive intermediates within the nitrogen cycle include (among others) nitrite, nitric oxide, and nitrous oxide, and studies examining the role and reactivity of these species are becoming more prevalent (Bange et al., 1996; Sun et al., 2017).

Table 1
Isotope Effects for Parameterization of Reaction-Diffusion Model, Differing by Model Scenario for Nitrate Reduction

Process	Isotope effect	Value (‰) sc. 1	Value (‰) sc. 2	References
Nitrite oxidation	$^{15}\varepsilon_{NXR}$	−15		Casciotti (2009)
	$^{18}\varepsilon_{NXR}$	−3		Buchwald and Casciotti (2010)
Nitrite reduction	$^{15}\varepsilon_{NIR}$	20		Martin and Casciotti (2016)
	$^{18}\varepsilon_{NIR}$	2		Martin and Casciotti (2016)
Ammonia oxidation	$^{15}\varepsilon_{AMO}$	15		Santoro et al. (2011)
	$^{18}\varepsilon_{O2}$	0		Buchwald et al. (2012)
	$^{18}\varepsilon_{H2O}$	15		Buchwald et al. (2012)
Nitrate reduction	$^{15}\varepsilon_{NAR}$	**25**	**60**[a]	Granger et al. (2008)
	$^{18}\varepsilon_{NAR}$	**25**	**35**[a]	Granger et al. (2008)
	$^{18}\varepsilon_{NAP}$, Branching	**−25**	**−35**[a]	Granger et al. (2008)

Note. Bold emphasis denotes values that are different between scenarios 1 and 2.
[a]Determined based on model fit; see section 4.1.

While concentrations alone reflect the net result of both production and consumption, naturally occurring stable isotopes provide a uniquely integrated and more comprehensive perspective on the total set of reactions. For example, the coupled stable isotopes of N (expressed in delta notation in units of per mil, (‰) where $\delta^{15}N = [(^{15}N/^{14}N_{sample}/(^{15}N/^{14}N_{air}) - 1] * 1{,}000)$ and O (expressed similarly, where $\delta^{18}O = [(^{18}O/^{16}O_{sample}/^{18}O/^{16}O_{VSMOW}) - 1] * 1{,}000$) of nitrate and nitrite (NO_2^-) can be used to identify areas in which nitrification and denitrification co-occur. Isotopic methods have been applied to water column oxygen deficient zones (ODZs; e.g., Buchwald et al., 2015) as well as deep-sea sediment profiles (e.g., Wankel et al., 2015) indicating an apparent overlap of reductive and oxidative processes at redox boundaries. While the modeling approaches are similar to those when using concentrations alone, known isotopic fractionation occurring between isotopologues (e.g., $^{14}NO_3^-$ vs. $^{15}NO_3^-$) also allows discrete estimation of rates of nitrification, nitrate reduction, and nitrite reduction. In addition, abiotic oxygen isotope equilibration processes can be used to constrain residence times of equilibrium-sensitive species, for example, nitrite (Buchwald & Casciotti, 2013).

Here we present pore water isotope data from the oligotrophic North Atlantic, combining perspectives from both nitrate and nitrite dual isotopic compositions (e.g., $\delta^{15}N$ and $\delta^{18}O$), spanning a redox gradient from fully oxic conditions at the sediment-water interface down to total depletion of oxygen and nitrate. Using a 1-D, reaction-diffusion model, we calculate depth-resolved estimates of rates of major N cycling processes, incorporating known isotope systematics of ammonia oxidation, nitrite oxidation, nitrate reduction, nitrite reduction, and oxygen isotope exchange between nitrite and water (Table 1 and Figure 1). We find evidence for the persistence of nitrite oxidation under anaerobic conditions and/or an unusually large discrepancy in the coupling of O and N isotope effects of nitrate reduction ($^{18}\varepsilon$:$^{15}\varepsilon$) distinct from those of canonical denitrification. Additionally, large differences observed between the $\delta^{15}N$ of nitrite and nitrate may also be explained by a uniquely prominent role for the reversible enzyme nitrite oxidoreductase (Freitag et al., 1987; Sundermeyer-Klinger et al., 1984; Tanaka et al., 1983). We discuss these alternative explanations for the observed isotopic data in the context of low-carbon environments, with possible implications for nitrogen cycling isotope dynamics in the broader biosphere.

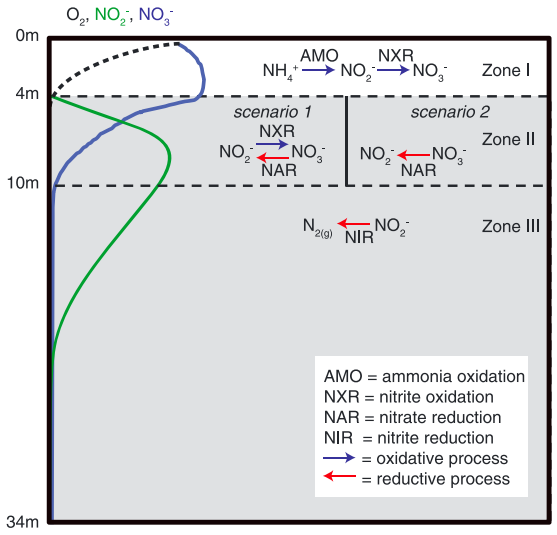

Figure 1. Schematic showing the distribution of processes evaluated using the 1-D reaction-diffusion model among three discrete depth zones: ammonia oxidation (AMO), nitrite oxidation (NXR), nitrate reduction (NAR), and nitrite reduction (NIR). The two model scenarios differ, by which processes are included in zone II (see text for details). Depths where oxygen concentrations are below detection (deeper than 4 mbsf) are shaded gray throughout this study.

While these findings lead to a significant improvement in our understanding of nitrogen cycling, they also demonstrate the need for a much deeper understanding of microbial metabolism across redox gradients. Our observations are similar to distributions observed in most ODZs of the global ocean and, given the extent of seafloor typified by similar sediments, provide a globally representative characterization of N cycling in redox gradients of sediments across ocean basins. Beyond oligotrophic sedimentary systems, these findings have further implications for the nature of N redox cycling and isotope budgets in many other systems, including ocean ODZs, coastal sediments, and estuarine environments.

2. Materials and Methods

2.1. Sample Collection

Samples were collected aboard the R/V *Knorr* using its long coring system in November of 2014 on cruise KN-223 in the North Atlantic. Samples used in this study came from two sediment coring sites located within 90 m of each other at 50°37.25′W, 14°24.05′N and 4,455-m water depth and are hereafter treated as one location (Figure 2). Pore waters were extracted at approximately 0.5-m intervals from two long piston

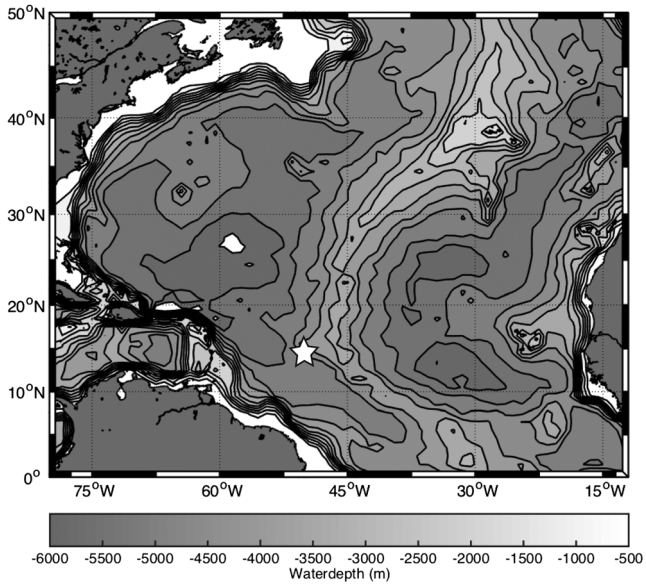

Figure 2. Map of pore water sampling location (star) with water depth contours.

cores (30 and 34 m long) using Rhizon™ samplers (0.2-μm pore size) and either analyzed shipboard or frozen until analyses were conducted shore side.

2.2. Pore Water Chemistry and Isotope Measurements

Nitrate and nitrite concentrations were determined shipboard using ion chromatography with UV detection (D'Hondt et al., 2015). Isotopes were measured in the Wankel lab (Woods Hole Oceanographic Institution) using an Isoprime 100 isotope ratio mass spectrometer coupled to a modified TraceGas prep system similar to that described previously (McIlvin & Casciotti, 2011), which is used to flush, purify, and cryogenically trap sample N_2O from converted nitrate or nitrite samples. Nitrate isotopic composition was measured using the denitrifier method to convert nitrate to N_2O, normalized to international reference materials (USGS 34, USGS 32, and USGS 35) (Casciotti et al., 2002; Sigman et al., 2001). Nitrite isotope measurements were made separately using the azide method for conversion of nitrite to N_2O (McIlvin & Altabet, 2005), normalizing to previously calibrated Wankel isotope lab standards (WILIS 10, 11, and 20) (Buchwald et al., 2016). Where co-occurring nitrite concentrations were less than 5 times as high as nitrate, nitrite was removed by addition of sulfamic acid (Granger & Sigman, 2009) prior to the denitrifier method. In the deepest samples having measurable nitrate, where concentrations were very low, the N and O isotopic composition of nitrate was calculated by mass balance using analyses of the combined nitrate + nitrite pools by the denitrifier method, in which both nitrate and nitrite standards were also analyzed, together with nitrite isotope values from the azide-only measurements described previously (Casciotti & McIlvin, 2007).

2.3. One-Dimensional Reaction-Diffusion Model Structure

We determined the rates of primary nitrogen cycling processes using an inverse 1-D reaction-diffusion model based on our measured vertical profiles of nitrate and nitrite concentrations and their corresponding $\delta^{15}N$ and $\delta^{18}O$ values (Buchwald et al., 2015). In addition to molecular diffusion, the model includes four major microbial transformation processes: ammonia oxidation, nitrite oxidation, nitrite reduction, and nitrate reduction (Figure 1). Also included in the model is the equilibration of nitrite oxygen isotopes with ambient water, with a reaction half-life of 50 days under ambient conditions of these sediments (Buchwald & Casciotti, 2013). The model minimizes the difference between predicted and measured values of eight different isotopologues, four for nitrate and four for nitrite: $^{14}NO_2^-$, $^{15}NO_2^-$, $N^{16}O_2^-$, $N^{18}O_2^-$, $^{14}NO_3^-$, $^{15}NO_3^-$, $N^{16}O_3^-$, and $N^{18}O_3^-$. The sum of both N isotopologues ($^{14}NO_2^-$ + $^{15}NO_2^-$ or $^{14}NO_3^-$ + $^{15}NO_3^-$) is equal to the measured concentration ($[NO_2^-]$ or $[NO_3^-]$) at any particular depth. The sum of the two oxygen isotopologues, divided by the number of oxygen atoms in each, is equal to the concentration of nitrite ($[NO_2^-] = (N^{16}O_2^- + N^{18}O_2^-)/2$) or nitrate ($[NO_3^-] = (N^{16}O_3^- + N^{18}O_3^-)/3$). The eight differential equations, which represent the time-dependent transformations and 1-D diffusion of these species, are given in Appendix A.

Central to the utility of this approach is the parameterization of the isotope effects associated with each of the N transformations, including those associated with oxygen incorporation during oxidation reactions and the $\delta^{18}O$ composition of these precursor O pools (i.e., water or O_2; see discussion). To solve the underdetermined system of equations, we choose fixed values for isotope effects and the initial isotopic composition of nitrate and nitrite during model initiation. The model is initialized with sediment pore fluid containing no nitrite and no nitrate. The model is run until nitrite and nitrate concentration profiles reach steady state.

Reaction rates were determined by dividing the vertical profiles into three major intervals based primarily on observed reactant concentrations (particularly O_2 and NO_3^-). Zone I includes the seawater interface and is dictated by the depth of O_2 penetration (to 4 meters below sea floor (mbsf)), while Zone III begins at the maximum depth of NO_3^- presence and extends downward and Zone II falls between these (Figure 1). Steady

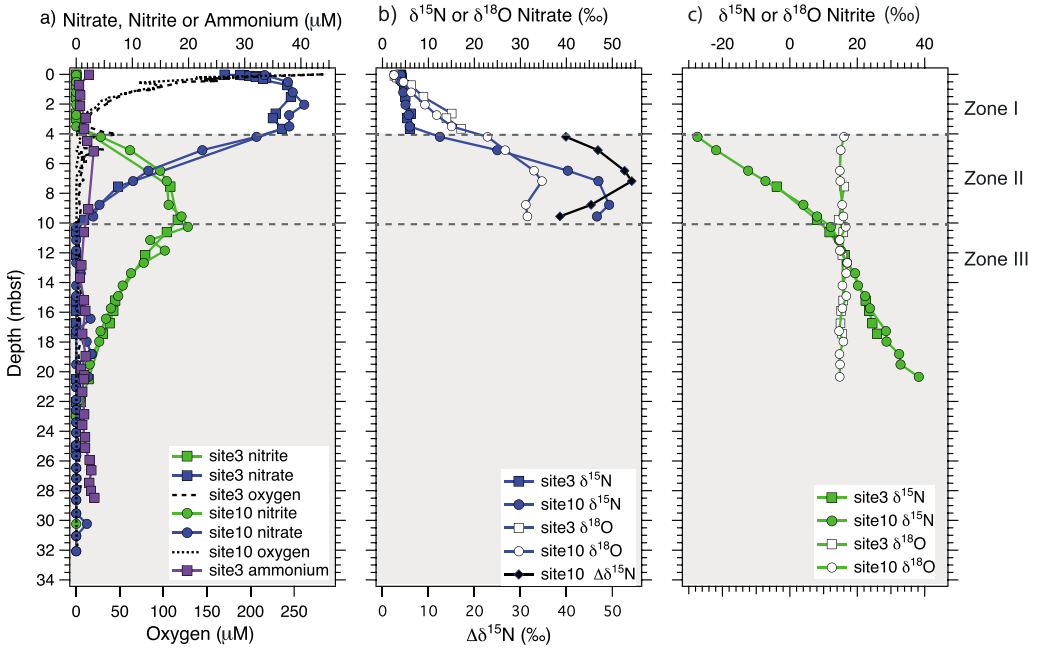

Figure 3. (a) Pore water concentrations of nitrate, nitrite, ammonium, and dissolved oxygen; (b) stable N and O isotope profiles for nitrate, including the difference in the $\delta^{15}N$ values of nitrate and nitrite ($\Delta\delta^{15}N = \delta^{15}N_{NO3} - \delta^{15}N_{NO2}$); and (c) the stable N and O isotope profiles for nitrite. The gray shaded area indicates oxygen concentration below detection limit (deeper than 4mbsf).

state reaction rates are determined by finding the combination of rate constants that best fits the distributions of all isotopologues and are optimized using a cost-fitting function (Appendix B). Two model scenarios are performed to examine different nitrate reduction isotope effects, while the isotope effects associated with ammonia oxidation and nitrite oxidation and reduction are held constant (Table 1).

3. Results

3.1. Nitrate and Nitrite Concentration and Stable Isotope Profiles

Concentration profiles of nitrate, nitrite, ammonium, and oxygen, as well as stable isotope profiles ($\delta^{15}N$ and $\delta^{18}O$) of nitrite and nitrate, are shown in Figure 3a. Bottom water in this region of the North Atlantic has a nitrate concentration of 23 μM (Marconi et al., 2014) and oxygen concentration of 280 μM (measured on cruise). Moving downward into the sediments, oxygen is mostly removed by 4 mbsf and absent (< 0.01 μM) by 7m bsf (Figure 3a). Nitrate increases to concentrations as high as 40 μM within the upper 4 mbsf and is completely removed by 10 mbsf. Nitrite, which is absent in the uppermost sediment column, begins to appear at ~4 mbsf, increasing to a maximum of 20 μM at 10 mbsf and dropping to below detection by 23 mbsf (Figure 3a).

Both $\delta^{15}N_{NO3}$ and $\delta^{18}O_{NO3}$ increase with depth into the sediment column (Figure 3b). Above 4 mbsf, where O_2 is measurable, the increase in $\delta^{15}N$ is distinctly muted compared to the corresponding increase in $\delta^{18}O$, corresponding to a $\Delta\delta^{18}O{:}\Delta\delta^{15}N$ of approximately 6.0 in this zone of net NO_3^- accumulation. In contrast, below the depth of O_2 disappearance, the observed decrease in NO_3^- concentration is associated with an increase in $\delta^{15}N$ that outpaces the increase in $\delta^{18}O$, manifesting as a $\Delta\delta^{18}O{:}\Delta\delta^{15}N$ of ~0.3.

Nitrite isotope profiles exhibit three distinct features (Figure 3c). First, $\delta^{18}O_{NO2}$ is essentially invariant throughout the profile, averaging +15.5‰ with a standard deviation of ±0.8‰. Second, in stark contrast to $\delta^{18}O_{NO2}$, $\delta^{15}N_{NO2}$ spans a range of nearly 70‰, with values as low as −28‰ in the shallowest nitrite sample, and increases steeply with depth up to values as high as +40‰ just before nitrite levels fall below detection. Third, a distinct change in the $\delta^{15}N$ slope with depth coincides with the NO_2^- concentration maximum and disappearance of nitrate at 10 mbsf.

4. Discussion

The concentration profiles of oxygen, nitrate, and nitrite from this site underlying the oligotrophic North Atlantic follow the same patterns as in other locations, such as continental shelf sediments, but extend over a much larger depth range as the result of lower microbial respiration rates. Here instead of oxygen depletion occurring over millimeters or centimeters, as in organic rich sediments, oxygen persists to ~4 mbsf. After oxygen is depleted there remains enough carbon to support heterotrophic nitrate reduction. After nitrate, nitrite then becomes the principal terminal electron acceptor from 10 to 23 mbsf. While the concentration profiles may suggest that the pore waters here follow a classic progression of redox reactions (Claypool & Kaplan, 1974; Froelich et al., 1979; Stumm & Morgan, 1996), the isotope profiles reveal a more complex story.

This unique data set includes well-resolved, high-resolution concentration and isotope profiles with a large accumulation of intermediate nitrite and no resolvable fluid advection (based on chloride profiles). Therefore, this data set offers a unique chance to shed light on the inner workings of nitrogen turnover across spatially broad redox gradients. The detailed understanding developed from the data from this site has important implications for N cycling in other aquatic environments including the ODZs of the global ocean. Below, using the 1-D reaction-diffusion model described above, we calculate depth-resolved rates of N transformations, explore possible mechanisms for reconciling several apparent puzzles, and discuss their implications for N cycling in other environments.

4.1. Nitrate Production in the Surface Sediments and the $\delta^{18}O_{NO3}$ Versus $\delta^{15}N_{NO3}$ (0 to 4 mbsf)

Within the oxic sediment of the upper 4 mbsf, the increase in NO_3^- concentrations above bottom water levels, a commonly observed feature in sediment pore water profiles, unequivocally reflects nitrate production through nitrification (ammonia oxidation followed by nitrite oxidation; Berelson et al., 1990; Goloway & Bender, 1982; Grundmanis & Murray, 1982; Hammond et al., 1996; Wankel et al., 2015). The conspicuous lack of nitrite accumulation indicates that the second step of nitrite oxidation is not rate limiting. The NO_3^- isotope profiles reflect a mixture of bottom water NO_3^- and regenerated NO_3^- (produced in situ by nitrification) in concert with the diffusive transport of these *end members*.

Bottom water NO_3^- in this region of the North Atlantic has a $\delta^{15}N$ value of +4.8‰ and a $\delta^{18}O$ value of +1.8‰ (Marconi et al., 2014). In the absence of NH_4^+ or NO_2^- accumulation, the $\delta^{15}N$ of regenerated NO_3^- should reflect the $\delta^{15}N$ of the organic matter supplied to the sediment. Nitrate $\delta^{15}N$ is almost constant with a slight increase with depth in this zone of remineralization and nitrification. By comparison, the $\delta^{18}O$ of regenerated NO_3^- reflects a combination of the isotopic composition of oxygen source molecules (water and dissolved O_2), as modified by kinetic isotope effects associated with their incorporation into product NO_3^- (Buchwald et al., 2012; Buchwald & Casciotti, 2010).

While water column $\delta^{18}O_{H2O}$ and $\delta^{18}O_{O2}$ can be assumed constant at approximately 0‰ and +24.1‰ (where in equilibrium with the atmosphere), respectively, this assumption is not necessarily applicable to the pore water environment. The persistent decrease in sediment pore water O_2 reflects consumption by respiration, a process with an isotopic fractionation effect that increases $\delta^{18}O_{O2}$ (Lane & Dole, 1956). Figure 4 shows calculated values of $\delta^{18}O_{O2}$ with depth, assuming a respiration isotope effect of either 13‰ (Angert et al., 2001; Kroopnick & Craig, 1976) or 20‰ (Kiddon et al., 1993; Kroopnick, 1975). In turn, to the degree that O_2 atoms are incorporated into newly produced NO_3^-, these elevated $\delta^{18}O_{O2}$ values will impact the $\delta^{18}O_{NO3}$ of regenerated NO_3^- produced through pore water-hosted nitrification (Figure 4). The impact that $\delta^{18}O_{O2}$ has on the $\delta^{18}O_{NO3}$ of newly produced NO_3^- depends on the extent of oxygen isotope equilibration between intermediate NO_2^- and ambient water, which has been estimated to vary between 0% and 25% (Casciotti et al., 2010). Oxygen isotope exchange between water and nitrite occurs abiotically at a rate related to temperature and salinity (Buchwald & Casciotti, 2013). In the conditions present here the half-life of this equilibration is predicted to be ~50 days. At equilibrium, the equilibrium isotope effect ($^{18}\varepsilon_{eq}$) reflects the $\delta^{18}O$ offset of nitrite above that of ambient water, here by about 14.8 to 15.7‰ for pore waters of 10 to 2 °C (Buchwald & Casciotti, 2013; Casciotti et al., 2007). In Zone I, where nitrite does not accumulate, we assume abiotic isotopic exchange is negligible (Buchwald et al., 2012). Figure 4 also includes the predicted $\delta^{18}O_{NO3}$ for regenerated NO_3^- with up to 50% water-derived O, which dampens the influence of the incorporation of enriched $\delta^{18}O_{O2}$, but also increases the $\delta^{18}O_{NO3}$

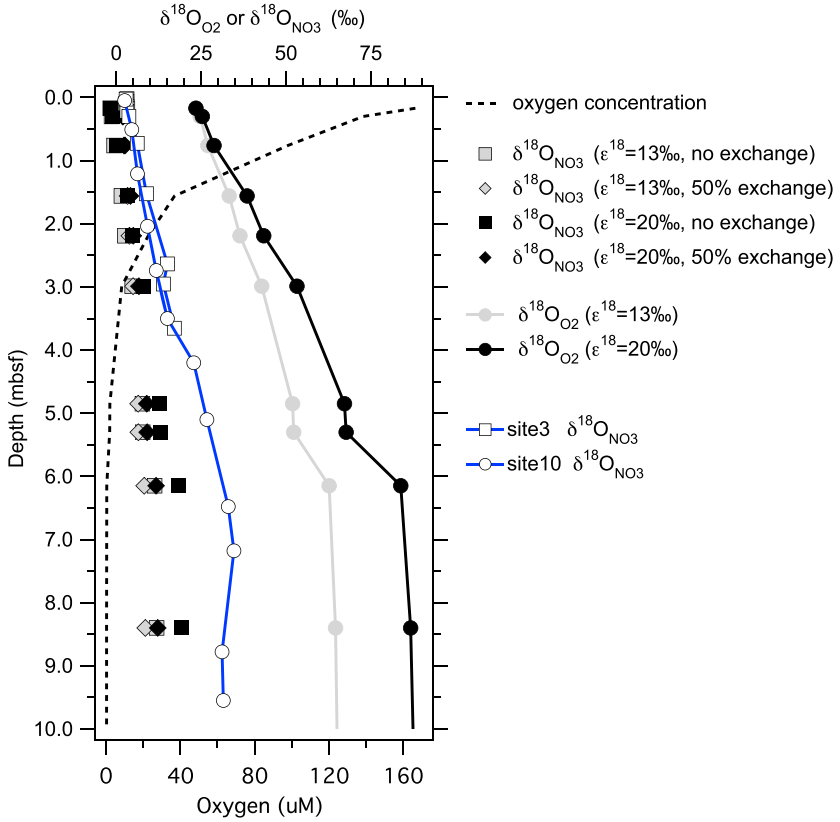

Figure 4. Measured oxygen concentration profile, measured nitrate $\delta^{18}O$, and model-estimated $\delta^{18}O$ of dissolved O_2 (based on two different isotope effects during respiration: 13‰ and 20‰) and the fraction of newly produced NO_3^- by nitrification (with and without 50% water-derived O).

as the result of the equilibrium isotope effect. Sigman et al. (2009) similarly concluded that the mean value of ocean nitrate is similar to the nitrification source (NO_2^-) $\delta^{18}O$, suggesting little influence by oxygen isotopic exchange during production of regenerated NO_3^-. Indeed, the incorporation of isotopically enriched O from fractionated O_2 into the newly nitrified pore water NO_3^- pool causes an increase in $\delta^{18}O$ relative to $\delta^{15}N$ (Figures 4 and 5). Equilibration of nitrite oxygen isotopes with water also contributes to the preferential increase in $\delta^{18}O$ relative to $\delta^{15}N$. Both of these processes, fractionation during O_2 incorporation and abiotic oxygen exchange between nitrite and water, together can easily account for the strong increase in $\delta^{18}O_{NO3}$ and the observed extreme $\delta^{18}O_{NO3}$ versus $\delta^{15}N_{NO3}$ slope of ~6 (Figure 5).

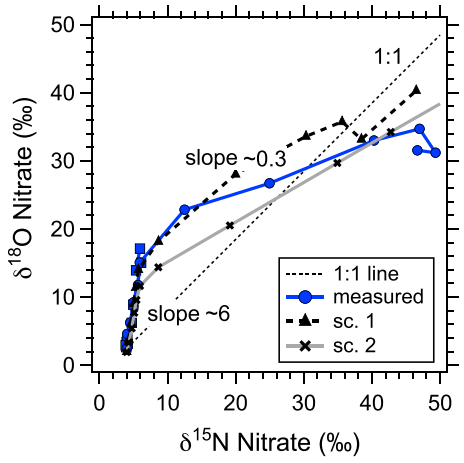

Figure 5. Measured nitrate $\delta^{15}N$ and $\delta^{18}O$ (blue circles) shown with a 1:1 line (dashed) anchored in the composition of bottom seawater. The 1:1 reference line is useful for evaluating the amount of denitrification, which should exhibit equal changes in $\delta^{15}N$ and $\delta^{18}O$ as NO_3^- is consumed. The nitrate isotope results for the two model scenarios described in Table 1 are shown.

4.2. Coupled Nitrification and Denitrification in the Shallow Anoxic Zone as Evidenced by the Shifting Relationship Between $\delta^{18}O_{NO3}$ and $\delta^{15}N_{NO3}$ as Well as $\Delta\delta^{15}N$ (5 to 10 mbsf)

Below the depth of O_2 penetration (Zone II; 5 to 10 mbsf), the onset of NO_2^- (and NH_4^+) accumulation (Figure 3) and the clear shift in the $\delta^{18}O_{NO3}$:$\delta^{15}N_{NO3}$ trend (Figure 5) reflect fundamental changes in the types and magnitudes of microbial nitrogen redox transformations. Nitrate isotopic composition in this zone is characterized by a strong increase in $\delta^{15}N_{NO3}$ values with depth, that, in contrast to those in Zone I, outpaces the corresponding increase in $\delta^{18}O_{NO3}$. In addition, $\delta^{15}N_{NO2}$ values in

this interval are exceptionally low, reaching as low as −28‰. In the absence of O_2, net nitrification is not expected to occur and organic matter oxidation is supported by nitrate reduction (Anderson et al., 1982).

The transition in metabolic N cycling regimes is easily seen in the evolving trend of coupled NO_3^- isotope compositions ($\delta^{18}O_{NO3}$:$\delta^{15}N_{NO3}$) depicted in Figure 5. While the slope of $\delta^{18}O$ versus $\delta^{15}N$ is very high in the oxygenated surface zone (~6), it drops dramatically to ~0.3 in this deeper zone. This pattern reflects a starkly different balance of processes affecting NO_3^- in the absence of dissolved O_2, conditions that poise denitrification as the most energy yielding respiratory pathway. Typically, values of $^{18}\varepsilon$ and $^{15}\varepsilon$ are strongly coupled (near 1:1) as measured in studies of denitrifying bacterial cultures utilizing respiratory nitrate reductase (NAR) (Granger et al., 2008). Here below the depth of O_2 penetration, however, the dramatic decrease in the $\delta^{18}O$ versus $\delta^{15}N$ trend, falling well below the 1:1 relation expected from unidirectional consumption by respiratory nitrate reductase, must reflect the influence of other more cryptic metabolic processes that are not directly observable with concentration data.

To further explain this transition, we turn to the dynamics of NO_2^-; below the depth of O_2 penetration, NO_2^- accumulation neatly tracks the disappearance of NO_3^-. The production of NO_2^- by NO_3^- reduction is generally associated with a large isotope effect ($^{15}\varepsilon_{NAR}$), yielding $\delta^{15}N_{NO2}$ values lower than the $\delta^{15}N$ of coexisting NO_3^- by approximately the value of $^{15}\varepsilon_{NAR}$. Indeed, $\delta^{15}N_{NO2}$ values in the zone of nitrite production are much lower than the coexisting nitrate at a given depth; yet the differences between the $\delta^{15}N$ of coexisting NO_2^- and NO_3^- ($\Delta\delta^{15}N = \delta^{15}N_{NO3} - \delta^{15}N_{NO2}$), up to 54‰ (Figure 3b), far exceed any published values for observed $^{15}\varepsilon_{NAR}$ in cultures of denitrifying bacteria (Granger et al., 2008). Notably, similarly large $\Delta\delta^{15}N$ values have been observed in isotope profiles from ODZs and have been largely ascribed to the cryptic reoxidation of nitrite occurring in the apparent absence of available O_2 (Altabet et al., 2012; Buchwald et al., 2015; Casciotti et al., 2013; Gaye et al., 2013). This dynamic arises because NO_2^- oxidation is associated with an inverse isotope effect that drives the $\delta^{15}N$ of the product NO_3^- higher while decreasing the $\delta^{15}N$ of residual NO_2^- beyond values expected to result from NO_3^- reduction alone (Casciotti, 2009).

4.3. Nitrite Reduction in the Deep Anoxic Zone (10 to 26 mbsf)

Finally, once NO_3^- has been completely consumed by nitrate reduction, the N isotope dynamics of NO_2^- are closely linked to its disappearance, presumably as the result of reduction coupled to organic matter respiration (e.g., denitrification; Figure 3). In this case, and in the presumed absence of any other processes producing nitrite, the increase in $\delta^{15}N_{NO2}$ directly reflects the isotope effect for nitrite reduction ($^{15}\varepsilon_{NIR}$) of the microbial community, a value of −21.6 ‰ using a fit to a first-order closed system model (not shown). This value indicates a likely dominance of copper-containing nitrite reductase (nirK) with limited contributions from iron-containing nitrite reductase (nirS), as it has been shown that nirS imparts a $^{15}\varepsilon_{NIR}$ of −8 ± 2‰, while nirK yields a $^{15}\varepsilon_{NIR}$ of −22 ± 2‰ (Martin & Casciotti, 2016).

4.4. Distribution of Nitrogen Transformation Rates

Calculated rates from the inverse 1-D reaction-diffusion model framework are shown in Figure 6. In the first model scenario (sc. 1; Figure 6), isotope effects are prescribed using representative values chosen from the literature (Table 1) and the model solves for rates of ammonia oxidation, nitrite oxidation and reduction, and nitrate reduction. A distinguishing characteristic of the results of this model scenario is the occurrence of nitrite oxidation in the absence of measurable O_2. In the second model scenario (sc. 2), isotopic fractionation of nitrate is treated as an unknown and optimized with a cost-fit function, while nitrite oxidation is set to zero below the O_2 penetration depth (Zones II & III). This approach allows us to illustrate the sensitivity of these parameters and examine inconsistencies between the modeled and measured isotope profiles that occur when a conventional redox zonation is assumed.

Estimated nitrogen transformation rates vary strongly as a function of depth through the sediment column (Figure 6e). Ammonia oxidation is predicted to occur at a constant prescribed rate of 0.02 μM NH_4^+ yr^{-1} in the top 4 meters of sediment where oxygen is present. The rate of ammonia oxidation was determined by the closest-fit model results to the measured NO_3^- concentration profile

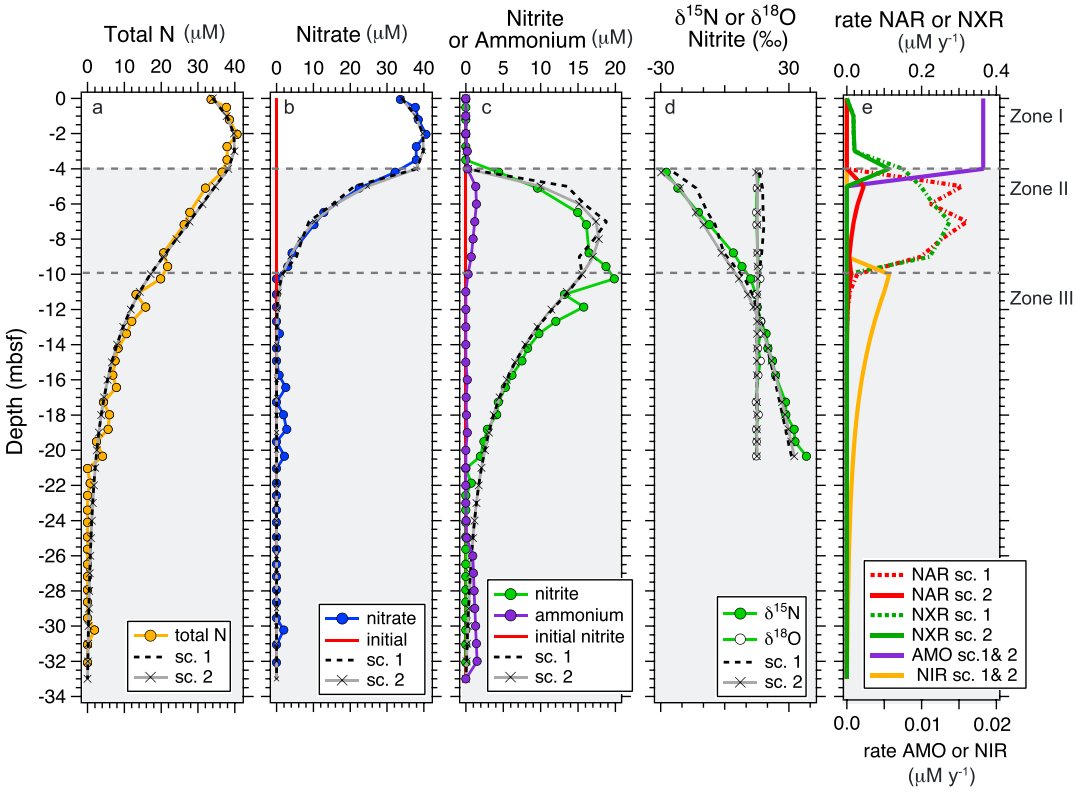

Figure 6. Measured profiles (colored lines) and corresponding model fits (gray and black dashed lines) for two scenarios (sc. 1 and sc. 2): (a) total inorganic nitrogen ($NH_4^+ + NO_3^- + NO_2^-$) concentration (N); (b) nitrate concentration; (c) nitrite and ammonium concentration; (d) nitrite N and O isotopic composition ($\delta^{15}N$ and $\delta^{18}O$); and (e) rate profiles for nitrate reduction (NAR, red), nitrite reduction (NIR, orange), nitrite oxidation (NXR, green), and ammonia oxidation (AMO, purple). Rates of ammonia oxidation and nitrite reduction are the same for both model scenarios. The only difference in sc. 1 and sc. 2 are the isotope effects for nitrate reduction, indicated in Table 1. The gray shaded region shows where oxygen is below detection (deeper than 4 mbsf).

of the upper 4 mbsf (Zone I), while ensuring that the net production of NO_3^- occurred without accumulation of NH_4^+ or NO_2^- (Figures 6b and 6e). It was assumed that nitrification was the only source of nitrate in the top 4 meters of sediment. At the lower boundary of Zone I, where O_2 is nearly depleted, nitrate reduction rates increase, with a maximum of 0.3 μM NO_3^- yr^{-1} at 7 mbsf. Nitrite oxidation also increases in close connection with nitrate reduction rates. Both nitrite oxidation and nitrate reduction rates are zero below 10 mbsf (Figure 6e). The total nitrogen profile indicates that nitrite reduction, the only process that removes fixed nitrogen, occurs only in the deepest zone (Zone III) (Figure 6e). Nitrite reduction exhibits maximum rates of 0.005 μM yr^{-1} tied to the highest nitrite concentration in the top of Zone III at 10 mbsf before tapering off in connection with the decay of nitrite with depth at 26 mbsf. Here again, a first-order rate constant was determined by optimizing the model to most closely reproduce the disappearance of total N with depth. While ammonia oxidation and nitrite reduction rates were primarily tied to the concentration profiles, rates of nitrate reduction and nitrite oxidation (Zone II) were more tightly constrained by the isotope profile distributions. Below we discuss how the relationship between nitrate $\delta^{15}N$ and $\delta^{18}O$, as well as the difference in $\delta^{15}N$ between nitrite and nitrate, influence the model solutions for nitrate reduction and nitrite oxidation.

4.5. Comparison to Previous Studies and Possible Mechanisms of Nitrite Reoxidation

As introduced above, the initial model parameterization yields rates of nitrate reduction and nitrite oxidation that track each other over the vertical extent of this zone (6 to 10 mbsf), with the fastest rates predicted at 0.3 μM y^{-1} at a depth of 7 mbsf. These rates of nitrate reduction are much lower than

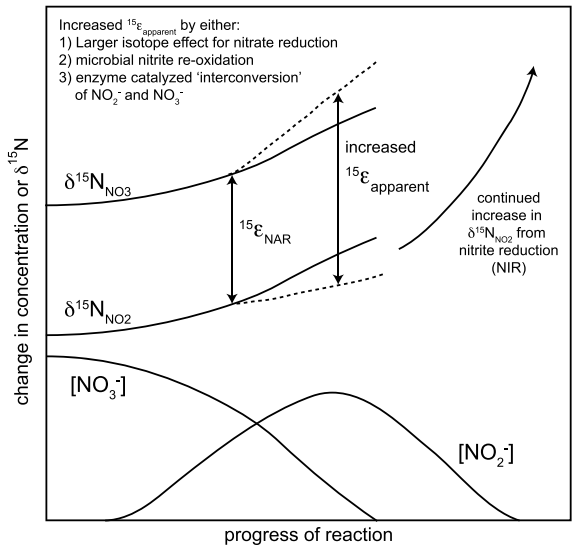

Figure 7. A schematic showing two different scenarios for the change in $\delta^{15}N$ of nitrate and nitrite during nitrate reduction. The solid line occurs when $\delta^{15}N$ difference between nitrite and nitrate is equal to the isotope effect for nitrate reduction, and the dotted line shows an increase in the $\delta^{15}N$ difference caused by three possible mechanisms, as described in the inset.

values measured in sediment and the water column in Eastern Tropical Pacific waters (Buchwald et al., 2015; Peters et al., 2016; Ward et al., 2009) and other oligotrophic sediments from the North Atlantic at North Pond (Wankel et al., 2015). Nitrite oxidation rates here are also lower than values observed in ODZs (~3 μM y^{-1}; (Buchwald et al., 2015)), but closer to water column values than other sediment environments. Nitrite oxidation rates are much lower (4 to 5 orders of magnitude) than values measured in coastal sediments (2.2 e^4 to 9.8 e^4 μM y^{-1}; (e.g., (Brin et al., 2014)). The values for nitrite oxidation in this study (up to 0.3 μM y^{-1}) equate to a residence time for nitrite of ~70 years. A long nitrite residence time is also supported by the $\delta^{18}O$ values of nitrite, which appear fully equilibrated with the $\delta^{18}O$ of water (Figure 3).

The co-occurrence of nitrite oxidation and nitrate reduction is a particularly important inference in this model. Although nitrite oxidation by nitrite-oxidizing bacteria (NOBs) in culture is only known to occur when linked to direct use of O_2, the reoxidation of nitrite under ostensibly anoxic conditions appears to be the only mechanism that is able to reconcile the dual isotope profiles of both NO_3^- and NO_2^- (Figures 3b and 3c). Indeed, it is this large turnover of nitrite and nitrate that presumably leads to the strong decrease in the slope of $\delta^{18}O_{NO3}$ versus $\delta^{15}N_{NO3}$ in this depth interval (Granger & Wankel, 2016). First, the $\delta^{15}N_{NO3}$ produced by nitrification is always higher than the value of $\delta^{15}N_{NO3}$ removed through nitrate reduction. Second, if $\delta^{18}O_{NO3}$ is greater than $\delta^{18}O_{H2O}$, as occurs here, then the $\delta^{18}O_{NO3}$ removed through nitrate reduction is greater than what is added through nitrification, also contributing to a decrease in the $\Delta\delta^{18}O_{NO3}$:$\Delta\delta^{15}N_{NO3}$. Lastly, enzyme-promoted equilibration of the $\delta^{18}O$ of water with nitrate during nitrification would also cause the small increase in $\delta^{18}O$ relative to $\delta^{15}N$ of NO_3^- (Buchwald & Casciotti, 2010; Casciotti et al., 2010; DiSpirito & Hooper, 1986; Friedman et al., 1986).

This reoxidation dynamic has been invoked in other zones where NO_2^- accumulation occurs, particularly in ODZs of the global ocean (Beman et al., 2013; Buchwald et al., 2015; Füssel et al., 2012; Martin & Casciotti, 2017; Peters et al., 2016). Indeed, reoxidation of nitrite under anoxic conditions, while still not well understood, may underpin a greater part of the natural nitrogen cycle than previously recognized (Babbin et al., 2017; Granger & Wankel, 2016; Sun et al., 2017). For example, recent studies have suggested that the larger than expected $\Delta\delta^{15}N$ values may actually be representative of isotopic equilibration between nitrite and nitrate, occurring in connection with highly reversible enzymatic activity (Figure 3b). This was first demonstrated in cultures of anammox bacteria, where the $\delta^{15}N$ of the nitrate produced was ~60‰ greater than the coexisting nitrite $\delta^{15}N$ (Brunner et al., 2013). We have included a schematic that illustrates a scenario, as in these pore waters, where the $\Delta\delta^{15}N$ increases over the expected value for the nitrate reduction isotope effect during nitrate removal (Figure 7). Nitrite reoxidation and other processes that will be described below can explain this increase.

To examine the requirement for such high levels of anaerobic nitrite reoxidation (e.g., nitrite-nitrate cycling), we adapted the model parameters to explicitly exclude any nitrite oxidation below the depth of O_2 penetration. In contrast to *sc. 1*, in which the co-occurrence of nitrate reduction and nitrite oxidation (with its strong inverse isotope effect) amplifies the accumulation of low $\delta^{15}N$ NO_2^-, this second configuration requires production of very low $\delta^{15}N$ nitrite directly from nitrate reduction. The resulting isotope effects of nitrate reduction that best explain the dual isotope profiles of NO_2^- and NO_3^- in Zone II are 60‰ and 35‰, for $^{15}\varepsilon_{NAR}$ and $^{18}\varepsilon_{NAR}$, respectively. *Sc. 2* also yielded lower overall rates of nitrate reduction in this zone (Figure 6). Notably, however, these fractionation values are far larger than those ever reported from studies of denitrifying and nitrate-reducing bacterial cultures (e.g., Granger et al., 2008). Thus, we are left with either a large oxidative flux of NO_2^- to NO_3^- under anoxic conditions, an apparent isotope effect for nitrate reduction that is much larger than any previous observation in bacterial cultures,

or the persistence of an enzyme-catalyzed isotope equilibrium occurring between NO_3^- and NO_2^-, which we discuss in more detail below.

4.6. Enzyme Level *Interconversion* as a Mechanism Contributing to Isotope Dynamics Between NO_3^- and NO_2^-

Under typical Earth surface conditions nitrite and nitrate nitrogen isotopes do not reach isotopic equilibrium, values of which have been estimated to fall near 55‰ (with $\delta^{15}N_{NO3} > \delta^{15}N_{NO2}$) (Casciotti, 2009). However, enzymatic reactions—especially those that are reversible—are well known to facilitate isotopic equilibrium in many different systems (Brunner et al., 2012; Sim et al., 2011; Yoshinaga et al., 2014). This phenomenon has not been widely investigated in the context of nitrogen cycling. However, nitrogen isotope equilibration between nitrate and nitrite was invoked recently as an explanation of isotope patterns observed in the surface Antarctic ocean (Kemeny et al., 2016), which the authors attributed to an enzymatically catalyzed *interconversion* by the reversible action of the nitrite oxidoreductase enzyme (NXR). In our study, however, it is difficult to invoke enzyme-catalyzed isotopic equilibrium using the same argument made for the surface Antarctic Ocean (Kemeny et al., 2016), in which the rapid transport of nitrite-oxidizing organisms into a *stressful* environment (high light and low nutrient surface ocean) was thought to initiate nitrite-nitrate interconversion by the reversibility of nitrite oxidoreductase. The same dynamic conditions clearly cannot be used to describe sediment-hosted organisms, which are generally subject to a quasi steady state with respect to their surroundings and available resources. While enzyme level interconversion has been suggested to occur in the surface Antarctic, and within cultures of anammox bacteria (Brunner et al., 2013), the exact mechanism causing the NXR enzyme to permit a reversible reaction and thereby promote isotopic equilibration is still unknown. Our data suggest that, despite limited oxygen availability, NOBs may persist at the thermodynamic threshold of nitrite oxidation (limited by O_2), which may lead to exceptionally high levels of enzyme-catalyzed isotope equilibration between nitrite and nitrate.

Similar arguments have been made for the distribution of carbon isotopes, for example, between methane and dissolved inorganic carbon near sulfate-methane transition zones, in which limitation of methane oxidation by low sulfate increases enzyme reversibility and leads to production of anomalously low carbon isotope compositions of methane as the result of an equilibrium distribution between methane and bicarbonate (Yoshinaga et al., 2014). Taken as a whole, the large apparent impact of NOBs (or other organisms with a reversible enzymatic pathway linking nitrate and nitrite) reflected by these pore water isotope compositions appears linked to their ability to compete with the carbon-limited heterotrophs requiring NO_3^- and NO_2^- for respiration. Thus, in these very low organic carbon environments, the reversibility of nitrite oxidoreductase, while still catalyzing a net forward oxidation of nitrite to nitrate, plays an unusually dominant role in the structure of the pore water isotopic profiles. Indeed, evidence for the persistence of NOBs in similarly low organic carbon marine sediments has been shown through pyrosequencing and qPCR, indicated by the presence of the NXR gene and NOBs throughout the sediment column across all levels of dissolved oxygen (S. Jørgensen, personal communication, 2014).

5. Conclusion

Our findings offer a unique perspective on the growing examination of coupled isotope measurements of nitrite and nitrate across other systems, including those in oceanic ODZs. Indeed, large differences in the $\delta^{15}N$ of nitrite and nitrate may be due in part to the complex and dynamic limitation of different microbial community members by the availability of resources including organic carbon, oxygen, nitrite, and nitrate. Future work in ODZs and other pore water settings should aim to better determine factors that may be regulating enzyme reversibility in nitrogen cycling with attention to implications for isotope systematics.

Appendix A: Equations Used in the 1-D Reaction Diffusion Model

The model used is a 1-D model that iterates over time (t) and depth (z). The time step (Δt) used was 1 year, which is then run for 100,000 years. The domain is set at 34 m, and each bin (Δz) is set at 1 m. Equations (A1)–(A8) represent the eight different parameters ($^{14}NO_2^-$, $^{15}NO_2^-$, $N^{16}O_2^-$, $N^{18}O_2^-$, $^{14}NO_3^-$, $^{15}NO_3^-$, $N^{16}O_3^-$, and $N^{18}O_3^-$). The concentration of nitrite [NO_2^-] is equal to ($^{14}NO_2 + {}^{15}NO_2^-$) or

Table A1
Initial Values for Isotopic Composition of Modeled Species

Isotope	Initial value (‰)
$\delta^{15}N_{nitrate,i}$	+4
$\delta^{18}O_{nitrate,i}$	+1.8
$\delta^{15}N_{nitrite,i}$	−20
$\delta^{18}O_{nitrite,i}$	+15
$\delta^{15}N_{ammonium}$	5
$\delta^{18}O_{H2O}$	0
$\delta^{18}O_{O2}$	23.5

($N^{16}O_2^- + N^{18}O_2^-$)/2, and the concentration of nitrate [NO_3^-] is equal to ($^{14}NO_3 + {}^{15}NO_3^-$) or ($N^{16}O_3^- + N^{18}O_3^-$)/3. Initial values for concentration and isotopic composition are shown in Table A1. Each parameter is transported by diffusion ($D = 0.01$ m^2/year and adjusted for each of the isotopes (D_{15NO2}, D_{N18O2}, D_{15NO3}, and D_{N18O3}) and is subject to biogeochemical processes of ammonia oxidation (AMO), nitrate reduction (NAR), nitrite reduction (NIR), and nitrite oxidation (NXR). The first-order rates of nitrate reduction (k_{NAR}), nitrite reduction (k_{NIR}), nitrite oxidation (k_{NXR}), the fractionation factors associated with N for the three processes ($^{15}\alpha_{NAR}$, $^{15}\alpha_{NIR}$, and $^{15}\alpha_{NXR}$), and the fractionation factors associated with O ($^{18}\alpha_{NAR}$, $^{18}\alpha_{NIR}$, $^{18}\alpha_{NXR}$, $^{18}\alpha_{EXCH}$, $^{18}\alpha_b$, $^{18}\alpha_{O2}$, and $^{18}\alpha_{H2O}$) are taken from the literature or fit by the model (Table 1). Ammonia oxidation is not modeled as first-order rate but instead as a total rate and also includes the fractionation factor, $^{15}\alpha_{AMO}$, from the literature. $^{18}\alpha_{EXCH}$ is the equilibrium isotope effect for the abiotic exchange of oxygen atoms between water and nitrite; $^{18}\alpha_b$ is the branching isotope fractionation, or kinetic isotope fractionation during the removal of one oxygen atom from nitrate during nitrate reduction; and $^{18}\alpha_{H2O}$ is the fractionation factor for the oxygen incorporation from water during nitrite oxidation. Isotope fractionation factors are shown in Table 1.

The system of centered difference equations where i is the index for time and j is the index for depth is as follows:

$$
{}^{14}NO_2^-(z_j,t_{i+1}) = {}^{14}NO_2^-(z_j,t_i) + \Delta t \begin{pmatrix} \frac{D}{\Delta z^2}\left({}^{14}NO_2^-(z_{j+1},t_i) - 2\,{}^{14}NO_2^-(z_j,t_i) + {}^{14}NO_2^-(z_{j-1},t_i)\right) \\ -k_{NXR}(z_j)\,{}^{14}NO_2^-(Z_j,t_i) \\ +k_{NAR}(z_j)\,{}^{14}NO_3^-(z_j,t_i) \\ -k_{NIR}(z_j)\,{}^{14}NO_2^-(z_j,t_i) \\ +\mathrm{rate}_{AMO}(z_j) \end{pmatrix} \tag{A1}
$$

$$
{}^{15}NO_2^-(z_j,t_{i+1}) = {}^{15}NO_2^-(z_j,t_i) + \Delta t \begin{pmatrix} \frac{D^* D_{{}^{15}NO_2^-}}{\Delta z^2}\left({}^{15}NO_2^-(z_{j+1},t_i) - 2\,{}^{15}NO_2^-(z_j,t_i) + {}^{15}NO_2^-(z_{j-1},t_i)\right) \\ -\frac{k_{NXR}(z_j)}{{}^{15}\alpha_{NXR}}\left({}^{15}NO_2^-(z_j,t_i)\right) \\ +\frac{k_{NAR}(z_j)}{{}^{15}\alpha_{NAR}}\left({}^{15}NO_3^-(z_j,t_i)\right) \\ -\frac{k_{NIR}(z_j)}{{}^{15}\alpha_{NIR}}\left({}^{15}NO_2^-(z_j,t_i)\right) \\ +\frac{\mathrm{rate}_{AMO}(z_j)}{{}^{15}\alpha_{AMO}} \end{pmatrix} \tag{A2}
$$

$$
N^{16}O_2^-(z_j,t_{i+1}) = N^{16}O_2^-(z_j,t_i) + \Delta t \begin{pmatrix} \frac{D}{\Delta z^2}\left(N^{16}O_2^-(z_{j+1},t_1) - 2N^{16}O_2^-(z_j,t_1) + N^{16}O_2^-(z_{j-1},t_1)\right) \\ -2k_{NXR}(z_j)\,{}^{14}NO_2^-(z_j,t_1) \\ +2k_{NAR}(z_j)\,{}^{14}NO_3(z_j,t_1) \\ -2k_{NIR}(z_j)\,{}^{14}NO_2^-(z_j,t_1) \\ +2\mathrm{rate}_{AMO}k_{AMO}(z_j) \end{pmatrix} \tag{A3}
$$

$$N^{18}O_2^-(z_j,t_{i+1}) = N^{18}O_2^-(z_j,t_i) + \Delta t \left(\begin{array}{l} \frac{D^* D_{N^{18}O_2^-}}{\Delta z^2}\left(N^{18}O_2^-(z_{j+1},t_i) - 2N^{18}O_2^-(z_j,t_i) + N^{18}O_2^-(z_{j-1},t_i)\right) \\ -\frac{k_{NXR}(z_j)}{{}^{18}\alpha_{NXR}}\left(N^{18}O_2^-(z_j,t_i)\right) \\ +k_{NAR}(z_j)\frac{2\left({}^{18}\alpha_{NAR}\right)}{3\left({}^{18}\alpha_b\right)}\left(N^{18}O_3^-(z_j,t_i)\right) \\ -\frac{k_{NIR}(z_j)}{{}^{18}\alpha_{NIR}}\left(N^{18}O_2^-(z_j,t_i)\right) \\ +\frac{\text{rate}_{AMO}(z_j)}{{}^{18}\alpha_{O_2}}\left(\delta\frac{{}^{18}O_{O_2}}{1,000}+1\right){}^{18}R_{VSMOW} \\ +\frac{\text{rate}_{AMO}(z_j)}{{}^{18}\alpha_{H_2O}}\left(\delta\frac{{}^{18}O_{H_2O}}{1,000}+1\right){}^{18}R_{VSMOW} \\ -k_{EXCH}(z_j)\left(N^{18}O_2^-(z_j,\ t_i)\right) \\ +k_{EXCH}(z_j)\left(N^{16}O_2^-(z_j,\ t_i)\right){}^{18}\alpha_{EXCH}\left(\frac{\delta^{18}O_{H_2O}}{1,000}+1\right){}^{18}R_{VSMOW} \end{array} \right) \quad \text{(A4)}$$

$${}^{14}NO_3^-(z_j,t_{i+1}) = {}^{14}NO_3^-(z_j,t_i) + \Delta t \left(\begin{array}{c} \frac{D}{\Delta z^2}\left({}^{14}NO_3^-(z_{j+1},t_i) - 2{}^{14}NO_3^-(z_j,t_i) + {}^{14}NO_3^-(z_{j-1},t_i)\right) \\ +k_{NXR}(z_j){}^{14}NO_2^-(z_j,t_i) \\ -k_{NAR}(z_j){}^{14}NO_3^-(z_j,t_i) \end{array} \right) \quad \text{(A5)}$$

$${}^{15}NO_3^-(z_j,t_{i+1}) = {}^{15}NO_3^-(z_j,t_i) + \Delta t \left(\begin{array}{c} \frac{D^* D_{{}^{15}NO_3^-}}{\Delta z^2}\left({}^{15}NO_3^-(z_{j+1},t_i) - 2{}^{15}NO_3^-(z_j,t_i) + {}^{15}NO_3^-(z_{j-1},t_i)\right) \\ +\frac{k_{NXR}(z_j)}{{}^{15}\alpha_{NXR}}{}^{15}NO_2^-(z_j,t_i) \\ -\frac{k_{NXR}(z_j)}{{}^{15}\alpha_{NAR}}{}^{15}NO_3^-(z_j,t_i) \end{array} \right) \quad \text{(A6)}$$

$$N^{16}O_3^-(z_j,\ t_{i+1}) = N^{16}O_3^-(z_j,t_i) + \Delta t \left(\begin{array}{c} \frac{D}{\Delta z^2}\left({}^{16}NO_3{}^-(z_{j+1},t_i) - 2N^{16}O_3^-(z_j,t_i) + N^{16}O_3^-(z_{j-1},t_i)\right) \\ +3k_{NXR}(z_j){}^{14}NO_2^-(z_j,t_i) \\ -3k_{NXR}(z_j){}^{14}NO_3^-(z_j,t_i) \end{array} \right) \quad \text{(A7)}$$

$$N^{18}O_3^-(z_j,t_{i+1}) = N^{18}O_3^-(z_j,t_i) + \Delta t \left(\begin{array}{c} \frac{D^* D_{N^{18}NO_3^-}}{\Delta z^2}\left(N^{18}O_3^-(z_{j+1},t_i) - 2N^{18}O_3^-(z_j,t_i) + N^{18}O_3^-(z_{j-1},t_i)\right) \\ +\frac{k_{NAR}(z_j)}{{}^{18}\alpha_{NAR}}N^{18}O_3^-(z_j,t_i) \\ -\frac{k_{NXR}(z_j)}{{}^{18}\alpha_{NXR}}N^{18}O_3^-(z_j,t_i) \\ +\frac{k_{NXR}(z_j)}{{}^{18}\alpha_{H_2O}}N^{14}O_2^-(z_j,t_i)\left(\frac{\delta^{18}OH_2O}{1,000}+1\right){}^{18}R_{VSMOW} \end{array} \right) \quad \text{(A8)}$$

Appendix B: Cost Function

The cost function is the sum of the squared differences between the data and model for the number of data points (N), calculated for each of the six first-order variables (k = $[NO_2^-]$, $[NO_3^-]$, $\delta^{15}N_{NO2}$, $\delta^{18}O_{NO2}$, $\delta^{15}N_{NO3}$, and $\delta^{18}O_{NO3}$). The weight (W_k) is a scale factor applied to normalize the absolute magnitudes where they differ greatly between variables. The weights were determined using the mean of the data points, and some were adjusted by a factor of 10 until each of the variables had approximately equal costs.

$$\text{cost} = \sqrt{\sum_{k=1}^{6}\left(\sum_{j=1}^{N}\frac{\left(x_k^{\text{model}}(j) - x_k^{\text{meas}}(j)\right)^2}{N*W}\right)} \tag{A9}$$

Acknowledgments

Samples analyzed for this study were collected during the final expedition of the RV *Knorr*, KN223. The expedition would not have been possible without the captain and crew of the RV *Knorr* and the efforts of the shipboard science party. We would like to acknowledge Robert Pockalny for planning and facilitating the expedition. Inorganic geochemistry sample collection, processing, and analysis were performed shipboard by Arthur Spivack, Dennis Graham, Chloe Anderson, Emily Estes, Kira Homola, Claire McKinley, Theodore Present, and Justine Sauvage. Coring capabilities were provided by the Oregon State University and Woods Hole Oceanographic Institute Coring Facilities, directed and funded by the U. S. National Science Foundation (NSF) Ship Facilities Program. The cored materials and discrete samples from the expedition are curated and stored by the Marine Geological Samples Laboratory at the University of Rhode Island, codirected by Rebecca Robinson and Katherine Kelly and funded by the NSF Ocean Sciences Division. The nutrient and isotope data from pore waters in this study will be available at The Biological and Chemical Data Management Office (https://www.bco-dmo.org/project/567401). This project was partially funded by an NSF CDEBI postdoctoral fellowship to C. Buchwald. Portions of this material are based upon work supported while R. W. M. was serving at the National Science Foundation.

References

Altabet, M. A., Ryabenko, E., Stramma, L., Wallace, D. W. R., Frank, M., Grasse, P., & Lavik, G. (2012). An eddy-stimulated hotspot for fixed nitrogen-loss from the Peru oxygen minimum zone. *Biogeosciences*, *9*(12), 4897–4908. https://doi.org/10.5194/bg-9-4897-2012

Anderson, J. J., Okubo, A., Robbins, A. S., & Richards, F. A. (1982). A model for nitrate distributions in oceanic oxygen minimum zones. *Deep Sea Research Part A. Oceanographic Research Papers*, *29*, 1113–1140.

Angert, A., Luz, B., & Yakir, D. (2001). Fractionation of oxygen isotopes by respiration and diffusion in soils and its implications for the isotopic composition of atmospheric O_2. *Global Biogeochemical Cycles*, *15*(4), 871–880. https://doi.org/10.1029/2000GB001371

Babbin, A. R., Peters, B. D., Mordy, C. W., Widner, B., Casciotti, K. L., & Ward, B. B. (2017). Multiple metabolisms constrain the anaerobic nitrite budget in the eastern tropical South Pacific. *Global Biogeochemical Cycles*, *31*, 258–271. https://doi.org/10.1002/2016GB005407

Bange, H. W., Rapsomanikis, S., & Andreae, M. O. (1996). Nitrous oxide in coastal waters. *Global Biogeochemical Cycles*, *10*(1), 197–207. https://doi.org/10.1029/95GB03834

Beman, J. M., Leilei Shih, J., & Popp, B. N. (2013). Nitrite oxidation in the upper water column and oxygen minimum zone of the eastern tropical North Pacific Ocean. *The ISME Journal*, *7*(11), 2192–2205. https://doi.org/10.1038/ismej.2013.96

Berelson, W. M., Hammond, D. E., O'neill, D., Xu, X. m., Chin, C., & Zukin, J. (1990). Benthic fluxes and pore water studies from sediments of the central equatorial North Pacific: Nutrient diagenesis. *Geochimica et Cosmochimica Acta*, *54*, 3001–3012.

Berner, R. A. (1964). Distribution and diagenesis of sulfur in some sediments from the Gulf of California. *Marine Geology*, *1*(2), 117–140. https://doi.org/10.1016/0025-3227(64)90011-8

Berner R. A. (1980) Early diagenesis: A theoretical approach. Retrieved from http://books.google.com/books?id=weRFglCVBkUC&pgis=1

Boudreau, B. P. (1997). *Diagenetic models and their implementation*, *Modelling Transport and Reactions in Aquatic Sediments*. Berlin: Springer. https://doi.org/10.1007/978-3-642-60421-8

Brin, L. D., Giblin, A. E., & Rich, J. J. (2014). Environmental controls of anammox and denitrification in southern New England estuarine and shelf sediments. *Limnology and Oceanography*, *59*(3), 851–860. https://doi.org/10.4319/lo.2014.59.3.0851

Brunner, B., Contreras, S., Lehmann, M. F., Matantseva, O., Rollog, M., Kalvelage, T., et al. (2013). Nitrogen isotope effects induced by anammox bacteria. *Proceedings of the National Academy of Sciences of the United States of America*, *110*(47), 18,994–18,999. https://doi.org/10.1073/pnas.1310488110

Brunner, B., Einsiedl, F., Arnold, G. L., Müller, I., Templer, S., & Bernasconi, S. M. (2012). The reversibility of dissimilatory sulphate reduction and the cell-internal multi-step reduction of sulphite to sulphide: Insights from the oxygen isotope composition of sulphate. *Isotopes in Environmental and Health Studies*, *48*(1), 33–54. https://doi.org/10.1080/10256016.2011.608128

Buchwald, C., & Casciotti, K. L. (2010). Oxygen isotopic fractionation and exchange during bacterial nitrite oxidation. *Limnology and Oceanography*, *55*(3), 1064–1074. https://doi.org/10.4319/lo.2010.55.3.1064

Buchwald, C., & Casciotti, K. L. (2013). Isotopic ratios of nitrite as tracers of the sources and age of oceanic nitrite. *Nature Geoscience*, *6*(4), 308–313. https://doi.org/10.1038/ngeo1745

Buchwald, C., Grabb, K., Hansel, C. M., & Wankel, S. D. (2016). Constraining the role of iron in environmental nitrogen transformations: Dual stable isotope systematics of abiotic NO_2-reduction by Fe (II) and its production of N_2O. *Geochimica et Cosmochimica Acta*, *186*, 1–12. https://doi.org/10.1016/j.gca.2016.04.041

Buchwald, C., Santoro, A. E., McIlvin, M. R., & Casciotti, K. L. (2012). Oxygen isotopic composition of nitrate and nitrite produced by nitrifying cocultures and natural marine assemblages. *Limnology and Oceanography*, *57*(5), 1361–1375. https://doi.org/10.4319/lo.2012.57.5.1361

Buchwald, C., Santoro, A. E., Stanley, R. H. R., & Casciotti, K. L. (2015). Nitrogen cycling in the secondary nitrite maximum of the eastern tropical North Pacific off Costa Rica. *Global Biogeochemical Cycles*, *29*, 2061–2081. https://doi.org/10.1002/2015GB005187

Canfield, D. E., Stewart, F. J., Thamdrup, B., De Brabandere, L., Dalsgaard, T., Delong, E. F., et al. (2010). A cryptic sulfur cycle in oxygen-minimum-zone waters off the Chilean coast. *Science*, *330*(6009), 1375–1378. https://doi.org/10.1126/science.1196889

Casciotti, K. L. (2009). Inverse kinetic isotope fractionation during bacterial nitrite oxidation. *Geochimica et Cosmochimica Acta*, *73*(7), 2061–2076. https://doi.org/10.1016/j.gca.2008.12.022

Casciotti, K. L., Böhlke, J. K., McIlvin, M. R., Mroczkowski, S. J., & Hannon, J. E. (2007). Oxygen isotopes in nitrite: Analysis, calibration, and equilibration. *Analytical Chemistry*, *79*(6), 2427–2436. https://doi.org/10.1021/ac061598h

Casciotti, K. L., Buchwald, C., & McIlvin, M. (2013). Implications of nitrate and nitrite isotopic measurements for the mechanisms of nitrogen cycling in the Peru oxygen deficient zone. *Deep-Sea Research Part I: Oceanographic Research Papers*, *80*, 78–93. https://doi.org/10.1016/j.dsr.2013.05.017

Casciotti, K. L., McIlvin, M., & Buchwald, C. (2010). Oxygen isotopic exchange and fractionation during bacterial ammonia oxidation. *Limnology and Oceanography*, *55*(2), 753–762. https://doi.org/10.4319/lo.2009.55.2.0753

Casciotti, K. L., & McIlvin, M. R. (2007). Isotopic analyses of nitrate and nitrite from reference mixtures and application to eastern tropical North Pacific waters. *Marine Chemistry*, *107*(2), 184–201. https://doi.org/10.1016/j.marchem.2007.06.021

Casciotti, K. L., Sigman, D. M., Hastings, M. G., Böhlke, J. K., & Hilkert, A. (2002). Measurement of the oxygen isotopic composition of nitrate in seawater and freshwater using the denitrifier method. *Analytical Chemistry*, *74*(19), 4905–4912. https://doi.org/10.1021/ac020113w

Claypool, G. E., & Kaplan, I. R. (1974). The origin and distribution of methane in marine sediments. In *Natural gases in marine sediments* (pp. 99–139). Plenum, NY: Plenum Press. https://doi.org/10.1007/978-1-4684-2757-8_8

D'Hondt, S., Inagaki, F., Zarikian, C. A., Abrams, L. J., Dubois, N., Engelhardt, T., et al. (2015). Presence of oxygen and aerobic communities from sea floor to basement in deep-sea sediments. *Nature Geoscience*, *8*(4), 299–304. https://doi.org/10.1038/ngeo2387

D'Hondt, S., Jørgensen, B. B., Miller, D. J., Batzke, A., Blake, R., Cragg, B. A., et al. (2004). Distributions of microbial activities in deep subseafloor sediments. *Science*, *306*(5705), 2216–2221. https://doi.org/10.1126/science.1101155

D'Hondt, S., Spivack, A. J., Pockalny, R., Ferdelman, T. G., Fischer, J. P., Kallmeyer, J., et al. (2009). Subseafloor sedimentary life in the South Pacific gyre. *Proceedings of the National Academy of Sciences of the United States of America*, *106*(28), 11,651–11,656. https://doi.org/10.1073/pnas.0811793106

DiSpirito, A. A., & Hooper, A. B. (1986). Oxygen exchange between nitrate molecules during nitrite oxidation by *Nitrobacter*. *The Journal of Biological Chemistry*, *261*, 10,534–10,537.

Freitag, A., Rudert, M., & Bock, E. (1987). Growth of *Nitrobacter* by dissimilatoric nitrate reduction. *FEMS Microbiology Letters*, *48*(1-2), 105–109. https://doi.org/10.1111/j.1574-6968.1987.tb02524.x

Friedman, S. H., Massefski, W., & Hollocher, T. C. (1986). Catalysis of intermolecular oxygen atom transfer by nitrite dehydrogenase of *Nitrobacter* agilis. *The Journal of Biological Chemistry*, *261*, 10,538–10,543.

Froelich, P. N., Klinkhammer, G. P., Bender, M. L., Luedtke, N. A., Heath, G. R., Cullen, D., et al. (1979). Early oxidation of organic matter in pelagic sediments of the eastern equatorial Atlantic: Suboxic diagenesis. *Geochimica et Cosmochimica Acta*, *43*(7), 1075–1090. https://doi.org/10.1016/0016-7037(79)90095-4

Füssel, J., Lam, P., Lavik, G., Jensen, M. M., Holtappels, M., Günter, M., & Kuypers, M. M. M. (2012). Nitrite oxidation in the Namibian oxygen minimum zone. *The ISME Journal*, *6*(6), 1200–1209. https://doi.org/10.1038/ismej.2011.178

Gaye, B., Nagel, B., Dähnke, K., Rixen, T., & Emeis, K. C. (2013). Evidence of parallel denitrification and nitrite oxidation in the ODZ of the Arabian Sea from paired stable isotopes of nitrate and nitrite. *Global Biogeochemical Cycles*, *27*, 1059–1071. https://doi.org/10.1002/2011GB004115

Goloway, F., & Bender, M. (1982). Diagenetic models of interstitial nitrate profiles in deep sea suboxic sediments. *Limnology and Oceanography*, *27*(4), 624–638. https://doi.org/10.4319/lo.1982.27.4.0624

Granger, J., & Sigman, D. M. (2009). Removal of nitrite with sulfamic acid for nitrate N and O isotope analysis with the denitrifier method. *Rapid Communications in Mass Spectrometry*, *23*(23), 3753–3762. https://doi.org/10.1002/rcm.4307

Granger, J., Sigman, D. M., Lehmann, M. F., & Tortell, P. D. (2008). Nitrogen and oxygen isotope fractionation during dissimilatory nitrate reduction by denitrifying bacteria. *Limnology and Oceanography*, *53*(6), 2533–2545. https://doi.org/10.4319/lo.2008.53.6.2533

Granger, J., & Wankel, S. D. (2016). Isotopic overprinting of nitrification on denitrification as a ubiquitous and unifying feature of environmental nitrogen cycling. *Proceedings of the National Academy of Sciences of the United States of America*, *113*(42), E6391–E6400. https://doi.org/10.1073/pnas.1601383113

Grundmanis, V., & Murray, J. W. (1982). Aerobic respiration in pelagic marine sediments. *Geochimica et Cosmochimica Acta*, *46*(6), 1101–1120. https://doi.org/10.1016/0016-7037(82)90062-X

Hammond, D. E., McManus, J., Berelson, W. M., Kilgore, T. E., & Pope, R. H. (1996). Early diagenesis of organic material in equatorial Pacific sediments: Stoichiometry and kinetics. *Deep-Sea Research Part II: Topical Studies in Oceanography*, *43*(4-6), 1365–1412. https://doi.org/10.1016/0967-0645(96)00027-6

Hansel, C. M., Lentini, C. J., Tang, Y., Johnston, D. T., Wankel, S. D., & Jardine, P. M. (2015). Dominance of sulfur-fueled iron oxide reduction in low-sulfate freshwater sediments. *The ISME Journal*, *9*(11), 2400–2412. https://doi.org/10.1038/ismej.2015.50

Kappler, A., & Bryce, C. (2017). Cryptic biogeochemical cycles: Unravelling hidden redox reactions. *Environmental Microbiology*, *19*(3), 842–846. https://doi.org/10.1111/1462-2920.13687

Kemeny, P. C., Weigand, M. A., Zhang, R., Carter, B. R., Karsh, K. L., Fawcett, S. E., & Sigman, D. M. (2016). Enzyme-level interconversion of nitrate and nitrite in the fall mixed layer of the Antarctic Ocean. *Global Biogeochemical Cycles*, *30*, 1069–1085. https://doi.org/10.1002/2015GB005350

Kiddon, J., Bender, M. L., Orchardo, J., Caron, D. A., Goldman, J. C., & Dennett, M. (1993). Isotopic fractionation of oxygen by respiring marine organisms. *Global Biogeochemical Cycles*, *7*(3), 679–694. https://doi.org/10.1029/93GB01444

Kroopnick, P., & Craig, H. (1976). Oxygen isotope fractionation in dissolved oxygen in the deep sea. *Earth and Planetary Science Letters*, *32*(2), 375–388. https://doi.org/10.1016/0012-821X(76)90078-9

Kroopnick, P. M. (1975). Respiration, photosynthesis, and oxygen isotope fractionation in oceanic surface water. *Limnology and Oceanography*, *20*(6), 988–992. https://doi.org/10.4319/lo.1975.20.6.0988

Lane, G. A., & Dole, M. (1956). Fractionation of oxygen isotopes during respiration. *Science*, *123*(3197), 574–576. https://doi.org/10.1126/science.123.3197.574

Marconi, D., Weigand, M. A., Rafter, P. A., McIlvin, M. R., Forbes, M., Casciotti, K. L., & Sigman, D. M. (2014). Nitrate isotope distributions on the US GEOTRACES North Atlantic cross-basin section: Signals of polar nitrate sources and low latitude nitrogen cycling. *Marine Chemistry*, *177*, 143–156.

Martin, T. S., & Casciotti, K. L. (2016). Nitrogen and oxygen isotopic fractionation during microbial nitrite reduction. *Limnology and Oceanography*, *61*(3), 1134–1143. https://doi.org/10.1002/lno.10278

Martin, T. S., & Casciotti, K. L. (2017). Paired N and O isotopic analysis of nitrate and nitrite in the Arabian Sea oxygen deficient zone. *Deep Sea Research Part I: Oceanographic Research Papers*, *121*, 121–131. https://doi.org/10.1016/j.dsr.2017.01.002

McIlvin, M. R., & Altabet, M. A. (2005). Chemical conversion of nitrate and nitrite to nitrous oxide for nitrogen and oxygen isotopic analysis in freshwater and seawater. *Analytical Chemistry*, *77*(17), 5589–5595. https://doi.org/10.1021/ac050528s

McIlvin, M. R., & Casciotti, K. L. (2011). Technical updates to the bacterial method for nitrate isotopic analyses. *Analytical Chemistry*, *83*(5), 1850–1856. https://doi.org/10.1021/ac1028984

Orcutt, B. N., Wheat, C. G., Rouxel, O., Hulme, S., Edwards, K. J., & Bach, W. (2013). Oxygen consumption rates in subseafloor basaltic crust derived from a reaction transport model. *Nature Communications*, *4*(1). https://doi.org/10.1038/ncomms3539

Orsi, W. D., Edgcomb, V. P., Christman, G. D., & Biddle, J. F. (2013). Gene expression in the deep biosphere. *Nature*, *499*(7457), 205–208. https://doi.org/10.1038/nature12230

Peters, B. D., Babbin, A. R., Lettmann, K. A., Mordy, C. W., Ulloa, O., Ward, B. B., & Casciotti, K. L. (2016). Vertical modeling of the nitrogen cycle in the eastern tropical South Pacific oxygen deficient zone using high-resolution concentration and isotope measurements. *Global Biogeochemical Cycles*, *30*, 1661–1681. https://doi.org/10.1002/2016GB005415

Riedinger, N., Brunner, B., Krastel, S., Arnold, G. L., Wehrmann, L. M., Formolo, M. J., et al. (2017). Sulfur cycling in an iron oxide-dominated, dynamic marine depositional system: The Argentine continental margin. *Frontiers in Earth Science*, *5*. https://doi.org/10.3389/feart.2017.00033/full

Santoro, A. E., Buchwald, C., McIlvin, M. R., & Casciotti, K. L. (2011). Isotopic signature of N_2O produced by marine ammonia-oxidizing archaea. *Science*, *333*(6047), 1282–1285. https://doi.org/10.1126/science.1208239

Schrenk, M. O., Huber, J. A., & Edwards, K. J. (2010). Microbial provinces in the subseafloor. *Annual Review of Marine Science*, *2*(1), 279–304. https://doi.org/10.1146/annurev-marine-120308-081000

Sigman, D. M., Casciotti, K. L., Andreani, M., Barford, C., Galanter, M., & Böhlke, J. K. (2001). A bacterial method for the nitrogen isotopic analysis of nitrate in seawater and freshwater. *Analytical Chemistry*, *73*(17), 4145–4153. https://doi.org/10.1021/ac010088e

Sigman, D. M., DiFiore, P. J., Hain, M. P., Deutsch, C., Wang, Y., Karl, D. M., et al. (2009). The dual isotopes of deep nitrate as a constraint on the cycle and budget of oceanic fixed nitrogen. *Deep Sea Research Part I: Oceanographic Research Papers*, *56*(9), 1419–1439. https://doi.org/10.1016/j.dsr.2009.04.007

Sim, M. S., Bosak, T., & Shuhei, O. (2011). Large isotope fractionation does not require disproportionation. *Science*, *333*(6038), 74–77. https://doi.org/10.1126/science.1205103

Stumm, W., & Morgan, J. J. (1996). *Aquatic chemistry: Chemical equilibria and rates in natural waters*, (3rd ed.). New York: John Wiley.

Sun, X., Ji, Q., Jayakumar, A., & Ward, B. B. (2017). Dependence of nitrite oxidation on nitrite and oxygen in low-oxygen seawater. *Geophysical Research Letters*, *44*, 7883–7891. https://doi.org/10.1002/2017GL074355

Sundermeyer-Klinger, H., Meyer, W., Warninghoff, B., & Bock, E. (1984). Membrane-bound nitrite oxidoreductase of *Nitrobacter*: Evidence for a nitrate reductase system. *Archives of Microbiology*, *140*(2-3), 153–158. https://doi.org/10.1007/BF00454918

Tanaka, Y., Fukumori, Y., & Yamanaka, T. (1983). Purification of cytochrome a1c1from *Nitrobacter* agilis and characterization of nitrite oxidation system of the bacterium. *Archives of Microbiology*, *135*(4), 265–271. https://doi.org/10.1007/BF00413479

Wang, G., Spivack, A. J., Rutherford, S., Manor, U., & D'Hondt, S. (2008). Quantification of co-occurring reaction rates in deep subseafloor sediments. *Geochimica et Cosmochimica Acta*, *72*(14), 3479–3488. https://doi.org/10.1016/j.gca.2008.04.024

Wankel, S. D., Buchwald, C., Ziebis, W., Wenk, C. B., & Lehmann, M. F. (2015). Nitrogen cycling in the deep sedimentary biosphere: Nitrate isotopes in porewaters underlying the oligotrophic North Atlantic. *Biogeosciences*, *12*(24), 7483–7502. https://doi.org/10.5194/bg-12-7483-2015

Ward, B. B., Devol, A. H., Rich, J. J., Chang, B. X., Bulow, S. E., Naik, H., et al. (2009). Denitrification as the dominant nitrogen loss process in the Arabian Sea. *Nature*, *461*(7260), 78–81. https://doi.org/10.1038/nature08276

Ward, B. B., & Zafiriou, O. C. (1988). Nitrification and nitric oxide in the oxygen minimum of the eastern tropical North Pacific. *Deep Sea Research Part A Oceanographic Research Papers*, *35*(7), 1127–1142. https://doi.org/10.1016/0198-0149(88)90005-2

Yoshinaga, M. Y., Holler, T., Goldhammer, T., Wegener, G., Pohlman, J. W., Brunner, B., et al. (2014). Carbon isotope equilibration during sulphate-limited anaerobic oxidation of methane. *Nature Geoscience*, *7*(3), 190–194. https://doi.org/10.1038/ngeo2069

Ziebis, W., McManus, J., Ferdelman, T., Schmidt-Schierhorn, F., Bach, W., Muratli, J., et al. (2012). Interstitial fluid chemistry of sediments underlying the North Atlantic gyre and the influence of subsurface fluid flow. *Earth and Planetary Science Letters*, *323–324*, 79–91.